



CHORUS

This is the accepted manuscript made available via CHORUS. The article has been published as:

## Optimal local control of coherent dynamics in custom-made nanostructures

Thomas Blasi, Mario F. Borunda, Esa Räsänen, and Eric J. Heller

Phys. Rev. B **87**, 241303 — Published 13 June 2013

DOI: [10.1103/PhysRevB.87.241303](https://doi.org/10.1103/PhysRevB.87.241303)

# Optimal Local Control of Coherent Dynamics in Custom-Made Nanostructures

Thomas Blasi,<sup>1,2</sup> Mario F. Borunda,<sup>3,1,\*</sup> Esa Räsänen,<sup>4,5,1</sup> and Eric J. Heller<sup>1,6</sup>

<sup>1</sup>*Department of Physics, Harvard University, Cambridge, Massachusetts 02138, United States*

<sup>2</sup>*Physik Department, Technische Universität München, James-Frank-Str., 85747 Garching, Germany*

<sup>3</sup>*Department of Physics, Oklahoma State University, Stillwater, Oklahoma 74078, United States*

<sup>4</sup>*Department of Physics, Tampere University of Technology, FI-33101 Tampere, Finland*

<sup>5</sup>*Nanoscience Center, Department of Physics, University of Jyväskylä, FI-40014 Jyväskylä, Finland*

<sup>6</sup>*Department of Chemistry and Chemical Biology, Harvard University, Cambridge, Massachusetts 02138, United States*

We apply quantum optimal control theory to establish a local voltage-control scheme that operates in conjunction with the numerically exact solution of the time-dependent Schrödinger equation. The scheme is demonstrated for high-fidelity coherent control of electronic charge in semiconductor double quantum dots. We find tailored gate voltages in the viable gigahertz regime that drive the system to a desired charge configuration with  $> 99\%$  yield. The results could be immediately verified in experiments and would play an important role in applications towards solid-state quantum computing.

PACS numbers: 81.07.Ta, 73.63.Hs, 73.63.Kv, 73.21.La, 07.05.Tp

During the past decade, advances in the fabrication of custom-made nanostructures have allowed the observation and coherent control of single-electron dynamics in low-dimensional semiconductor systems improving the prospects and feasibility of quantum information processing<sup>1,2</sup>. In this context, electron transport through double quantum dots (DQDs) has been an active field of research<sup>3</sup> and opened access to controlling electron dynamics on the single particle level<sup>4</sup> as demonstrated by several groundbreaking experiments<sup>5–11</sup>. Fast and accurate control of electronic states is a key requirement for solid-state quantum information processing. Here we apply local optimal control theory (OCT), a powerful approach to find optimized gate voltages that induce coherent transitions between electronic states in solid-state devices. The proposed schemes achieve (i) faster operation time and (ii) limits the frequencies used in the voltage profile to the experimentally accessible range, while maximizing the fidelity of the process.

The behavior of electric charge in DQDs has recently been the subject of several theoretical studies proposing schemes to coherently control the dynamics of the electrons<sup>12–17</sup>. Theoretical strategies based on global gate voltages<sup>14,15</sup> and optimized laser pulses<sup>16,17</sup> have shown that it is possible to control the electronic states in DQD models. However, the fabrication of working devices would be easier if coupling to terahertz optical fields<sup>17</sup> or the use of strong gate voltages modulated in picosecond time-scales<sup>14,15</sup> was avoided. In this communication, we demonstrate an optimized method to control the single-electron dynamics in DQDs by applying local gate voltages. We employ OCT<sup>18,19</sup> to find optimized and realistic gigahertz voltage profiles enabling coherent single-electron transfer with extremely high fidelities. We apply OCT towards the optimization of local potentials to drive transitions from a delocalized to a localized electronic state. To the best of our knowledge, OCT has not been applied to obtain *local* time-dependent potentials

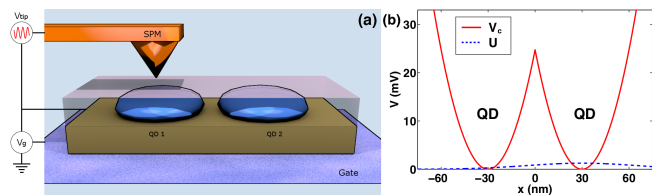


FIG. 1: Schematic of the double quantum dot system. (a) Two quantum dots are embedded in a semiconductor heterostructure. A back gate voltage  $V_g$  applied to the substrate can tune the global potential in the system. A local gate, such as the charged tip of a scanning probe microscope (SPM) capacitively coupled to the system, can change the potential locally. When the SPM tip is located above one of the quantum dots, applying a time-dependent voltage  $V_{tip}(t)$  induces a local time-dependent potential  $U(x,t)$  affecting mainly one of the dots. (b) Confinement potential  $V_c(x)$  for a one dimensional double quantum dot system and the potential  $U(x,t)$  induced by the local gate.

is solid-state devices before. We demonstrate the general applicability of our approach in one- and two-dimensional DQD systems.

As illustrated in Fig. 1(a), we consider a DQD system consisting of two quantum wells separated by a tunnel barrier with an additional time-dependent local potential  $U(x,t)$ . The local time-varying potential could be realized by using local gate voltages<sup>8</sup> that affect only one of the dots or the charged tip of a scanning probe microscope (SPM) acting as a local gate<sup>22,23</sup>. A voltage difference  $V_{tip}$  between the tip and the system would induce a charge  $q = CV_{tip}$  in the dot located underneath the SPM, where  $C$  is the capacitance between the tip and the dot. For the systems studied here, we consider GaAs material parameters within the effective-mass approximation, i.e.,  $m^* = 0.067m_e$  and  $\epsilon = 12.4\epsilon_0$ .

The time-dependent Hamiltonian is given by  $\mathcal{H}(x,t) = p^2/(2m^*) + V_c(x) + U(x,t)$ , where  $V_c(x)$  is the DQD

confinement potential (see below) and  $U(x, t)$  is described above [see Fig. 1(b)]. For gates that do not change position, the potential is separable and can be expressed as the product of the spatial and temporal parts,  $U(x, t) = g(x)f(t)$ . We model the spatial part as  $g(x) = (\beta/\sigma\sqrt{2\pi})\exp(-x^2/2\sigma^2)$  with  $\beta = 1.0$  nm and  $\sigma = 34.3$  nm.

Our goal is to find the optimal time-dependent function  $f(t)$  such that the electron wavefunction  $|\Psi(t)\rangle$  is driven from its initial state  $|\Psi(t=0)\rangle = |\Phi_I\rangle$  into a predefined target state  $|\Phi_F\rangle$ . The process concludes at a fixed target time  $T$ , when the overlap  $|\langle\Psi(T)|\Phi_F\rangle|^2$  is maximal. In contrast to conventional applications of OCT, where the controlling field is the dipole interaction resulting from applying a laser field (cf. Ref. 21), we use a local potential  $\mathcal{H}_{\text{loc}} = U(x, t)$  as the control field. The control equations now become

$$i\partial_t\Psi(t) = \mathcal{H}(t)\Psi(t), \quad \Psi(0) = \Phi_I \quad (1)$$

$$i\partial_t\chi(t) = \mathcal{H}(t)\chi(t), \quad \chi(T) = \Phi_F\langle\Phi_F|\Psi(T)\rangle \quad (2)$$

$$f(t) = -\frac{1}{\alpha}\text{Im}\langle\chi(t)|g(x)|\Psi(t)\rangle, \quad (3)$$

Equation (1) represents the Schrödinger equation and the initial conditions used while Eq. (2) is the time evolution of the system while the overlap  $\chi(T)$  is maximized. We set the fluence, a measure of the total irradiated energy presented here in units of [voltage<sup>2</sup> × time], to a fixed value  $\int_0^T dt f^2(t) = F^*$ . In Eq. (3) for the field, the Lagrange multiplier  $\alpha$  is calculated through the fixed fluence  $F^*$  as explained in detail in Ref. 21. To solve the control equations (1-3), we use the iterative method of Werschnik and Gross<sup>24</sup> and the split-operator method<sup>25</sup> for the time propagation implemented in the `octopus` code package<sup>26</sup>.

In principle, arbitrary charge states can be chosen for the initial and final state<sup>21</sup>. In the scenarios tested here, the chosen initial state is the ground state  $|\Phi_I\rangle = |1\rangle$  and the target state is a left localized electronic configuration  $|\Phi_F\rangle = |L\rangle$ . Each of those two states has a measurable signature which can be experimentally distinguished using charge sensing techniques<sup>27</sup>. Moreover, by setting  $f(t) = 0$  at  $t = 0$  and  $t = T$ , the local gate voltage  $U(x, t)$  is zero at the initial and final times, and the time evolution of the system after the control scheme has been applied remains unaltered. We note, that in the framework of QOCT it is also possible to require different envelope constraints on the envelope of  $f(t)$ <sup>21</sup>.

The states localized in a quantum well can be expressed as superpositions of the two lowest (symmetric and antisymmetric) states  $|1\rangle$  and  $|2\rangle$  by  $|L\rangle = 1/\sqrt{2}(|1\rangle - |2\rangle)$  and  $|R\rangle = 1/\sqrt{2}(|1\rangle + |2\rangle)$ . At  $t = T$ , once the system has reached either one of the superpositions, oscillations of frequency  $\omega_{12} = E_2 - E_1$  are induced between the occupation probabilities of  $|L\rangle$  and  $|R\rangle$ . Experimentally,

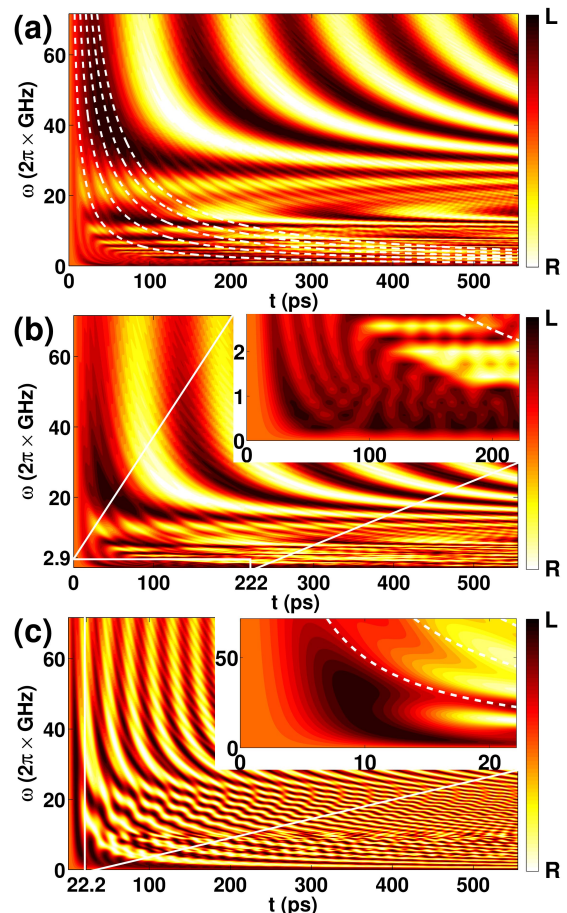


FIG. 2: Probability of the electron occupying the left or right well as a function of time and frequency of the time-dependent local gate voltage  $f(t) = A \sin(\omega t)$  acting only on the right well. Dashed lines correspond to  $f(t) = 0$ . Interdot distance is fixed at  $d = 58.7$  nm in all three plots. The confinement strength  $\omega_0$ , energy spacing  $\omega_{12}$ , and the field amplitude  $A$  are as follows: (a)  $\omega_0 = 2\pi \times 2.03$  THz,  $\omega_{12} = 2\pi \times 10.0$  GHz, and  $A = 11.9$  mV, (b)  $\omega_0 = 2\pi \times 2.03$  THz,  $\omega_{12} = 2\pi \times 10.0$  GHz, and  $A = 5.9$  mV, and (c)  $\omega_0 = 2\pi \times 1.43$  THz,  $\omega_{12} = 2\pi \times 38.7$  GHz, and  $A = 5.9$  mV. The insets highlight the optimization regimes used when limiting the parameters to (b) low frequencies ( $T = 222$  ps and a filter frequency  $\omega_{\text{max}} = 2\pi \times 2.87$  GHz) and (c) shorter local gate voltage interactions ( $T = 22.2$  ps and a filter frequency  $\omega_{\text{max}} = 2\pi \times 71.7$  GHz).

due to the presence of impurities, a local gate voltage would have to be applied to one of the wells of the DQD to render the left and right dots energetically degenerate.

We first consider a 1D system with confinement  $V_c^{1D}(x) = \omega_0^2/2 \min\{(x-d/2)^2, (x+d/2)^2\}$  [see Fig. 1(b)], where  $d$  is the interdot distance and  $\omega_0$  is the confinement strength. The general challenges in the control of such a harmonic system have been considered in Ref. 12. We investigate the localization of the electron when a monochromatic time-dependent gate voltage  $f(t) = A \sin(\omega t)$  is applied to one of the wells. Fig. 2 presents the degree of localization of the electron in the

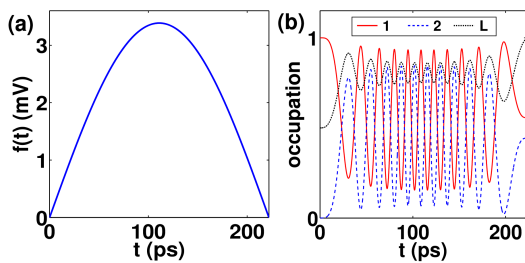


FIG. 3: Low-frequency optimization of the delocalized electron state to a left-localized state transition. The target state is reached while minimizing the frequencies of the local gate voltage to the few GHz frequency regime. (a) Shape of the optimal field obtained by applying OCT to the local gates for a pulse limited by a filter frequency to  $\omega_{\max} = 2\pi \times 2.87$  GHz and of duration  $T = 222$  ps. This pulse can be fit by the sinusoidal function  $f(t) = 3.55 \sin(2\pi \times 2.25 \text{GHz} \times t)$  mV. (b) Overlap of the wavefunction during the time evolution with the states  $|1\rangle$  (red) and  $|2\rangle$  (blue) as well as for the left-localized superposition  $|L\rangle$  (black). The target state is reached with a yield of 99.5%.

left (right) well as functions of time  $t$  and field frequency  $\omega$  for three sets of amplitudes for the gate voltage  $A$  and confinement strength of the wells  $\omega_0$ . Dashed lines indicate when the gate voltage is zero  $f(t) = 0$ , corresponding to  $\omega t = n\pi$  ( $n = 1, 2, \dots$ ). For clarity, only the lines for  $n \leq 5$  are depicted. The complex behavior seen in Fig. 2, especially at low frequencies, is a result of the combination of inherent system dynamics (oscillation of the superposition) and the system-field interaction. Overall, Fig. 2 demonstrates that electron localization is very sensitive to the amplitude and frequency. High-fidelity control thus calls for optimized schemes applied as follows. As will be shown, such a scheme does not necessarily lead to a complicated control gate voltage. In contrast, control schemes applied to *optical* fields have led to rather complicated pulses<sup>12,16,17</sup>.

For concreteness, we consider two optimized voltage profiles for local gates acting on the right quantum well that drive the system from the ground state to the left-localized configuration achieving maximum fidelity. We analyze the obtained fields by fitting them with a sum  $f(t) = \sum_i A_i \sin(\omega_i t + \varphi_i)$  and show that in spite of this simplification, the yield is not notably altered. This technique is both useful for experimental applicability and interesting in terms of robustness of the optimized fields calculated with QOCT<sup>28</sup>.

In Fig. 3 we present the optimization of a local gate voltage where the involved frequencies are limited to the low gigahertz regime. The parameters used for the optimization of the gate voltage of the 1D system with  $d = 58.7$  nm and  $\omega_0 = 2\pi \times 2.03$  GHz is limited to the region highlighted in the inset of Fig. 2(b). The maximum allowed frequency is  $\omega_{\max} = 2\pi \times 2.87$  GHz and the field duration is  $T = 222$  ps. The energy difference between the left- and right-localized state, determined by the width of the tunneling barrier, is  $\omega_{12} = 2\pi \times 10.0$

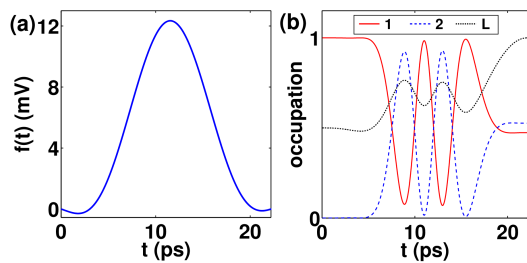


FIG. 4: Fast optimization of the delocalized electron state to a left-localized state transition. The target state is reached while minimizing the interaction time of the local gate voltage to a few picoseconds. (a) Shape of the optimal field obtained by applying OCT to the local gates for a pulse of duration  $T = 22.2$  ps and limited by a filter frequency to  $\omega_{\max} = 2\pi \times 71.7$  GHz. This pulse can be fit by a sum of two sinusoidal functions. (b) Overlap of the wavefunction during the time evolution with the states  $|1\rangle$  (red) and  $|2\rangle$  (blue) as well as for the left-localized superposition  $|L\rangle$  (black). The target state is reached with a yield of 99.9%.

GHz. By iterating the control equations, we find a field that achieves an extremely high overlap of 99.5%. The time dependence of the gate potential as well as the occupations of the states  $|1\rangle$ ,  $|2\rangle$  and their superposition  $|L\rangle$  are presented in Fig. 3. Due to the large energy difference between the second and third state ( $E_3 - E_2 = 1.96$  THz), the occupation of states  $n > 2$  remains zero during the process. Strikingly, the optimal field contains only one frequency  $\omega = 2\pi \times 2.25$  GHz. Thus, the optimal field can be well represented by the simple expression  $f(t) = A \sin(\omega t)$ , with  $A = 3.55$  mV. We point out, however, that due to the complexity of the low frequency dynamics (see Fig. 2), it would be a cumbersome task to determine the correct frequency *and* the amplitude without optimization. Yet, OCT provides a simple and experimentally feasible frequency/amplitude combination in a single computation.

To establish a faster delocalized-localized transition rate, we consider the parameter range in the inset of Fig. 2(c) and set  $\omega_0 = 2\pi \times 1.43$  THz,  $\omega_{\max} = 2\pi \times 71.7$  GHz, and  $T = 22.2$  ps. The energy difference between the first two states is  $\omega_{12} = 2\pi \times 38.7$  GHz. OCT produces the field presented in Fig. 4(a) resulting in 99.9% overlap. The optimal field can be reconstructed with two frequencies  $f(t) = A_1 \sin(\omega_1 t + \varphi_1) + A_2 \sin(\omega_2 t + \varphi_2)$  where  $\omega_1 = 2\pi \times 22.5$  GHz,  $\omega_2 = 2\pi \times 67.7$  GHz,  $A_1 = 9.36$  mV,  $A_2 = 3.64$  mV,  $\varphi_1 = -0.0713$ , and  $\varphi_2 = -3.32$ . As before, the reconstructed field keeps the yield unaltered.

Finally, we demonstrate that OCT applies also to 2D DQDs modeled here by a confining potential  $V_c^{2D}(x, y) = \max\{G(x - d_x) + G(x) + G(x + d_x), G(y - d_y) + G(y + d_y)\}$ , where  $G(x) = (a/c\sqrt{2\pi}) \exp(-x^2/2c^2)$  are Gaussian-shaped barriers that set the DQD size to  $2d_x = 68.5$  nm in the x-direction and  $2d_y = 34.3$  nm in the y-direction. The constants  $a$  and  $c$  control the height and width of the barriers: the full width at half maximum of the barrier is  $\text{FWHM} = 2\sqrt{2} \ln 2c = 4.90$  nm and its maximal

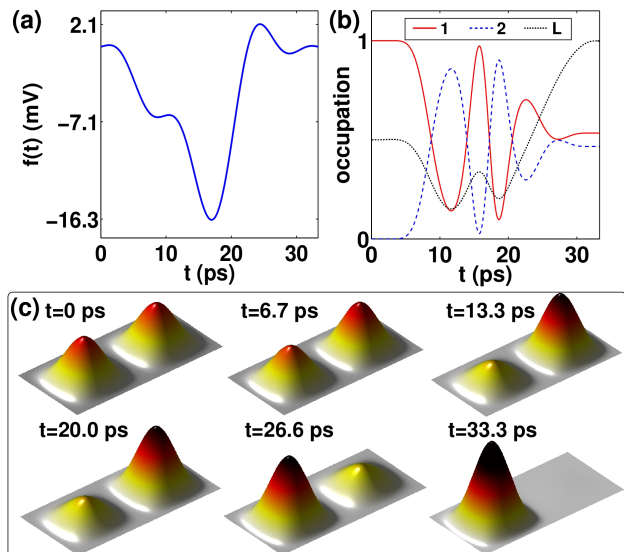


FIG. 5: Local gate OCT optimization of a two-dimensional system. The transition from a delocalized electron state to a left-localized state transition is achieved by minimizing the interaction time. (a) Shape of the optimal field obtained by applying OCT. The best fit for the pulse is given by  $f(t) = \sum_{i=1}^4 A_i \sin(\omega_i t + \varphi_i)$  with the parameters  $\omega_1 = 2\pi \times 15.0$  GHz,  $\omega_2 = 2\pi \times 45.0$  GHz,  $\omega_3 = 2\pi \times 75.1$  GHz,  $\omega_4 = 2\pi \times 105$  GHz,  $A_1 = 8.96$  mV,  $A_2 = 4.64$  mV,  $A_3 = 2.89$  mV,  $A_4 = 1.91$  mV,  $\varphi_1 = 0.234$ ,  $\varphi_2 = -2.71$ ,  $\varphi_3 = -0.443$ , and  $\varphi_4 = -3.77$ . (b) Overlap of the wave function during the time evolution with the states  $|1\rangle$  (red) and  $|2\rangle$  (blue) as well as for the left-localized superposition  $|L\rangle$  (black). (c) Snapshots of the probability density of the electron for several times. Initially the probability density is higher for the right dot while after 23 ps, it is more likely to find the electron on the left dot. Finally, when the local gate interaction is complete at  $T = 34.9$  ps, the target state is reached with a yield of 99.6%.

height is  $h_{\max} = a/c\sqrt{2\pi} = 178$  mV. The energy difference between the symmetric and antisymmetric state is  $E_2 - E_1 = 2\pi \times 26.5$  GHz. The use of OCT finds an optimized local gate voltage that contains frequencies below  $\omega_{\max} = 2\pi \times 115$  GHz, as presented in Fig. 5(a). The local gate acts in the 2D DQDs system for  $T = 34.9$  ps and drives the system into the left-localized state with a probability of 99.6% (Fig. 5(b)). Again, the pulse can be analyzed and successfully reconstructed without reducing the yield. The probability amplitude of the electron wave function is illustrated for several time steps in Fig. 5(c)<sup>29</sup>. Comparing our results to an approach, where the gate voltage is simply tuned up in an unoptimized way to an amplitude  $A$  (see Fig. 2), shows that the yields obtained with our method are at least 10 percentage points higher for the given target times.

This work shows that OCT can be used to pursue the goals of accelerating the target time  $T$  and/or minimizing the applied frequency range without compromising the fidelity of the process. To establish the practicality

of the experimental realization of the proposed control scheme, we discuss the robustness of our result in the presence of disorder and sensitivity to dephasing. First, the actual potential (including the contribution from impurities) of a particular quantum well can be obtained by inverting the Schrödinger equation for the measured single-electron spectrum<sup>30</sup>. Optimizing with the actual potential could then be done with OCT. The robustness of the control strategy should be assessed in the context of the Hamiltonian identification proposed above, where the accurate identification of the disorder potential is of great significance. We point out that the gigahertz regime is experimentally accessible and thus the obtained fields [see Figs. 3(a), 4(a), 5(a)] are realizable, in contrast to an instantaneous switching of the electric field<sup>15</sup>. The pulse sequence necessary for the control schemes are accomplished in a time scale that ranges from 22 ps to 222 ps. These times are below the inhomogeneous dephasing time of 250 ps measured by different techniques in GaAs DQDs at temperatures  $\sim 90$  mK<sup>11,31,32</sup>. Therefore, we believe that the time scales presented here are reachable.

In conclusion, we have shown through numerically exact calculations that electron localization in a single-electron semiconductor DQD system can be coherently controlled with simple but optimized local gate voltages up to extremely high fidelities. To this end, we have extended the application of quantum optimal control theory to the domain of local potentials. Our analysis has shown that the optimized local fields can be easily reconstructed in the gigahertz regime. The general applicability of our approach has been demonstrated by considering both one- and two-dimensional systems and different confining potentials. The demonstrated optimizations are obtained using physical constraints that are within reach of present experimental setups, resulting in an opportunity for a clean test of OCT. The coherent high-fidelity control of electronic charge via surface or back gates, or via the tip of a scanning probe microscope, represents a clear advancement in solid-state quantum information.

## I. ACKNOWLEDGEMENT

The authors thank Robert Westervelt, Alberto Castro, and Holger Hennig for helpful discussions. M.F.B. and E.J.H. were supported by the Department of Energy, office of basic science (grant DE-FG02-08ER46513), E.R. by the Academy of Finland, the European Community's FP7 through the CRONOS project, grant agreement no. 280879, the Wihuri Foundation, and the Magnus Ehrnrooth Foundation, and T.B. by the German National Academic Foundation. CSC Scientific Computing Ltd. in Finland and the Odyssey cluster supported by the FAS Science Division Research Computing Group at Harvard University are acknowledged for computational resources.

- 
- \* Electronic address: [mario.borunda@okstate.edu](mailto:mario.borunda@okstate.edu)
- <sup>1</sup> D. Loss and D. P. DiVincenzo, Phys. Rev. A **57**, 120 (1998).
  - <sup>2</sup> M. A. Nielsen and I. L. Chuang, *Quantum Computation and Quantum Information* (Cambridge Univ. Press, Cambridge, 2000).
  - <sup>3</sup> W. G. van der Wiel, S. De Franceschi, J. M. Elzerman, T. Fujisawa, S. Tarucha, and L. P. Kouwenhoven, Rev. Mod. Phys. **75**, 1 (2003).
  - <sup>4</sup> T. Fujisawa, T. Hayashi, and S. Sasaki, Rep. Prog. Phys. **69**, 759 (2006).
  - <sup>5</sup> T. Hayashi, T. Fujisawa, H. D. Cheong, Y. H. Jeong, and Y. Hirayama, Phys. Rev. Lett. **91**, 226804 (2003).
  - <sup>6</sup> J. R. Petta, A. C. Johnson, C. M. Marcus, M. P. Hanson, and A. C. Gossard, Phys. Rev. Lett. **93**, 186802 (2004).
  - <sup>7</sup> P. Fallahi, A. C. Bleszynski, R. M. Westervelt, J. Huang, J. D. Walls, E. J. Heller, M. P. Hanson, and A. C. Gossard, Nano Lett. **5**, 223 (2005).
  - <sup>8</sup> J. Gorman, D. G. Hasko and D. A. Williams, Phys. Rev. Lett. **95**, 090502 (2005).
  - <sup>9</sup> L. Robledo, J. Elzerman, G. Jundt, M. Atatüre, A. Högele, S. Fält, and A. Imamoglu, Science **320**, 772 (2008).
  - <sup>10</sup> M. Kataoka, M. R. Astley, A. L. Thorn, D. K. L. Oi, C. H. W. Barnes, C. J. B. Ford, D. Anderson, G. A. C. Jones, I. Farrer, D. A. Ritchie, and M. Pepper, Phys. Rev. Lett. **102**, 156801 (2009).
  - <sup>11</sup> K. D. Petersson, J. R. Petta, H. Lu, and A. C. Gossard, Phys. Rev. Lett. **105**, 246804 (2010).
  - <sup>12</sup> E. Räsänen, A. Castro, J. Werschnik, A. Rubio, and E. K. U. Gross, Phys. Rev. B **77**, 085324 (2008).
  - <sup>13</sup> L. Sælen, R. Nepstad, I. Degani, and J. P. Hansen, Phys. Rev. Lett. **100**, 046805 (2008).
  - <sup>14</sup> G. E. Murgida, D. A. Wisniacki, and P. I. Tamborenea, Phys. Rev. Lett. **99**, 036806 (2007).
  - <sup>15</sup> G. E. Murgida, D. A. Wisniacki, and P. I. Tamborenea, Phys. Rev. B **79**, 035326 (2009).
  - <sup>16</sup> A. Putaja and E. Räsänen, Phys. Rev. B **82**, 165336 (2010).
  - <sup>17</sup> E. Räsänen, T. Blasi, M. F. Borunda, E. J. Heller, Phys. Rev. B **86**, 205308 (2012).
  - <sup>18</sup> A. P. Peirce, M. A. Dahleh, and H. Rabitz, Phys. Rev. A **37**, 4950 (1988).
  - <sup>19</sup> R. Kosloff, S. A. Rice, P. Gaspard, S. Tersigni, and D. J. Tannor, Chem. Phys. **139**, 201 (1989).
  - <sup>20</sup> C. Brif, R. Chakrabarti, and H. Rabitz, New J. Phys. **12**, 075008 (2010).
  - <sup>21</sup> J. Werschnik and E. K. U. Gross, J. Phys. B: Atom. Mol. Opt. Phys. **40**, R175 (2007).
  - <sup>22</sup> A. C. Bleszynski, F. A. Zwanenborg, R. M. Westervelt, A. L. Roest, E. P. A. M. Bakkers, and L. P. Kouwenhoven, Nano Lett. **7**, 2559 (2007).
  - <sup>23</sup> E. E. Boyd; K. Storm, L. Samuelson, and R. M. Westervelt, Nanotechnology **22**, 185201 (2011).
  - <sup>24</sup> J. Werschnik and E. K. U. Gross, J. Opt. B: Quantum Semiclass. Opt. **7**, S300 (2005).
  - <sup>25</sup> M. D. Feit, J. A. Fleck, and A. Steiger, J. Comp. Phys. **47**, 412 (1982).
  - <sup>26</sup> A. Castro, H. Appel, M. Oliveira, C. A. Rozzi, X. Andrade, F. Lorenzen, M. A. L. Marques, E. K. U. Gross, and A. Rubio, Phys. Stat. Sol. (b) **243**, 2465 (2006).
  - <sup>27</sup> M. Field, C. G. Smith, M. Pepper, D. A. Ritchie, J. E. F. Frost, G. A. C. Jones, and D. G. Hasko, Phys. Rev. Lett. **70**, 1311 (1993).
  - <sup>28</sup> H. Rabitz, Phys. Rev. A **66**, 063405 (2002).
  - <sup>29</sup> See Supplemental Material at [URL will be inserted by publisher] for a schematic movie of the time evolution of the probability density presented in Fig. 5c.
  - <sup>30</sup> E. Räsänen, J. Könemann, R. J. Haug, M. J. Puska, and R. M. Nieminen, Phys. Rev. B **70**, 115308 (2004).
  - <sup>31</sup> Y. Dovzhenko, J. Stehlik, K. D. Petersson, J. R. Petta, H. Lu, and A. C. Gossard, Phys. Rev. B **84**, 161302(R) (2011).
  - <sup>32</sup> J. Stehlik, Y. Dovzhenko, J. R. Petta, J. R. Johansson, F. Nori, H. Lu, and A. C. Gossard, Phys. Rev. B **86**, 121303(R) (2012).